J Solid State Electrochem (2009) 13:1695–1700
DOI 10.1007/s10008-008-0635-y

ORIGINAL PAPER

Protective coatings for stainless steel for SOFC applications

S. Molin · B. Kusz · M. Gazda · P. Jasinski

Received: 13 May 2008 / Revised: 8 July 2008 / Accepted: 20 July 2008 / Published online: 8 August 2008

Abstract In this paper, a coating procedure based on spin coating of metal oxide polymer precursors on stainless steel, which decreases the oxide scale growth rate, is evaluated. The yttrium and cobalt solutions were used as polymer precursors, while a ferritic stainless steel Crofer 22 APU was used for the deposition of protective coatings. The thickness of deposited protective film was about ~500 nm. The effectiveness of protective layer was evaluated by cyclic thermogravimetry, oxide scale electrical conductivity, and X-ray diffractometry. The results show that steel coated with yttrium polymer precursor has better properties than uncoated or cobalt-coated sample.

Keywords Fuel cell · Corrosion · Coating · Oxidation

Introduction

Solid oxide fuel cells are one of the most prospective future energy sources [1–3]. Their successful commercialization depends mainly on lowering of their fabrication costs. Ceramic materials used as interconnectors for high-temperature solid oxide fuel cells (SOFC; 800–1,000 °C) are expensive and difficult for machining. Lowering the working temperature to 600–800 °C allows incorporating stainless steel, which significantly reduces SOFC costs. However, several problems exist when stainless steel wants to be used in SOFC, e.g., mismatch of thermal expansion coefficient between ceramic and steel, oxide scale formation, and chromia poisoning. Interconnector plate is in the same time exposed to a highly oxidizing air atmosphere on the cathode side and a highly reducing hydrogen atmosphere on the anode side of a fuel cell so that the successful candidate material must remain stable in both environments. Among steels, ferritic stainless steels gained the most attention due to their close matching of thermal expansion coefficients with ceramic materials used in SOFC [4]. High-temperature corrosion process, which occurs in all steels, results in oxide scale formation on the surface of the steel. The oxide scale can have low electronic conductivity, unmatched thermal expansion coefficient with steel or ceramic leading to spallation, or can react with ceramic functional layers. It is generally agreed that only chromia (Cr_2O_3)-forming alloys are regarded as prospective oxide scale [5]. Chromium oxide is a semiconductor and has a relatively high electronic conductivity in comparison to other possible protective scales: Al_2O_3, SiO_2. The continuous layer of chromia can be formed when the content of chromium is on the level of 17–20 wt.%. However, the chromia scale might poison cathodes by chromium gaseous species which evaporate from steel in humid air conditions [6]. Chromium evaporation can be avoided either by a bulk modification of steel or by application of a special protective coatings. Addition of small amounts of special alloying elements into steel might promote formation of other scale than chromia that will result in decreased chromium evaporation and enhanced electrical conductivity. For example, the Mn addition causes formation of

Presented at the international conference CORROSION TODAY held in Gdansk-Sobieszewo, Poland, 23 to 26 April 2008.

S. Molin (✉) · P. Jasinski
Faculty of Electronics, Telecommunication and Informatics,
Gdansk University of Technology,
ul.G. Narutowicza 11/12,
80-952 Gdansk, Poland
e-mail: molin@biomed.eti.pg.gda.pl

B. Kusz · M. Gazda
Faculty of Applied Physics and Mathematics,
Gdansk University of Technology,
ul.G. Narutowicza 11/12,
80-952 Gdansk, Poland

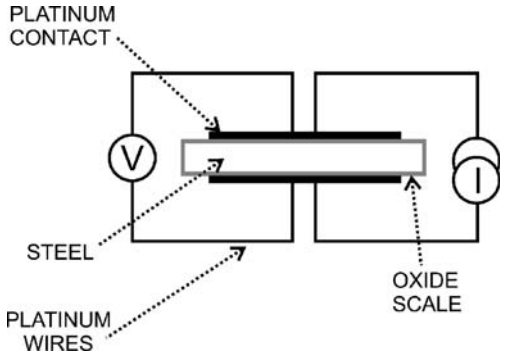

Fig. 1 Oxide scale electrical conductivity measurement setup

(Mn,Cr) spinel on the surface of steel and, in result, decreases the formation of volatile chromium species and improves electrical conductivity of the oxide scale [7, 8]. Recently, special protective coatings are used very extensively and provide similar results as bulk modification. They are easier to fabricate and test in laboratory conditions, so a variety of compositions can be checked. Especially, binary oxides and perovskites have been extensively studied. It was shown that single oxide reactive elements based on La, Y, Nd, Ce, and Co are very prospective materials [9–11]. The (La,Sr)MnO_3, (La,Sr)CrO_3, and (La,Sr)FeO_3 are perovskite materials which were investigated as well [12–15]. The deposition method used to coat substrates is an important factor. The results might vary due to some differences in deposition mechanism, e.g., physical or chemical. In addition, thickness of layers, heat treatment, and surface pretreatment can be visible experimental aspects. So far, mainly thick (>10 μm) coatings were evaluated [9]. Recently, due to the advancement in technology, some attention is given to thin films (~200 nm) [11, 16]. As an example, a successful thin protective oxide of (Mn,Co) spinel was deposited by a filtered arc plasma source ion deposition process [16], which resulted in the improvement of electrical conductivity of oxide scale and which remained stable (below 10 mΩ cm^2) in the 1,000-h measurement time at 800 °C.

In this paper, results of investigation of protective coatings of Y and Co on stainless steel are presented. The films were prepared by spin coating of polymer precursors. The properties of protective coating were evaluated by cyclic thermogravimetry and measurements of oxide scale conductivity. A ferritic Crofer 22 APU stainless steel is used in this study. It is a specially designed alloy for SOFC interconnector application which was developed in Research Center Juelich, Germany and manufactured by Thyssen Krupp VDM, Germany. The Crofer 22 APU is a chromia-forming alloy (~22% Cr) with small additives of other atoms (max. 0.8% Mn, max. 0.5% Si, max. 0.5% Cu, max. 0.2% La and Ti, max. 0.5% Al) to improve high-temperature performance.

Experiment

The Crofer 22 APU steel sheet was cut into 25×25×3-mm^3 coupons. Each side of the coupon was polished using silicon carbide sandpaper (from #120 to #1200 grit) to obtain clear and shiny surface. After polishing, samples were washed in acetone and deionized water in ultrasonic cleaner. Before coating, coupons were heated at 380 °C on a hot plate.

Metal oxide polymer precursors were prepared by dissolution of appropriate metal cations in deionized water (DI) and ethylene glycol (EG), which served as a polimerizable agent. For each precursor, 0.01 mol of metal salt was added to 20 ml of DI water and 40 ml of EG. The mixtures were then stirred on a hot plate at ~80 °C for about 12 h to expel water. The obtained precursors were viscous, and they properly wetted steel coupons. The ~0.25 M yttrium precursors were prepared from Y$(NO_3)_3 x 6H_2O$ (Aldrich), while ~0.25 M cobalt precursors from Co$(NO_3)_3 x 6H_2O$ (Aldrich).

Spin coating method was used to coat the samples with thin layer of polymer precursor. The maximum spinning rate of 2,500 rpm for 30 s was employed. Volume of mixture deposited on samples by a pipette was ~0.1 ml for each deposition. The coupons were coated 15 times on each side, and after each deposition, they were heated on a hot plate up to 380 °C to decompose organics and yield nanocrystalline ceramic film. The thickness of coatings is of about 30 nm per single deposition step as determined

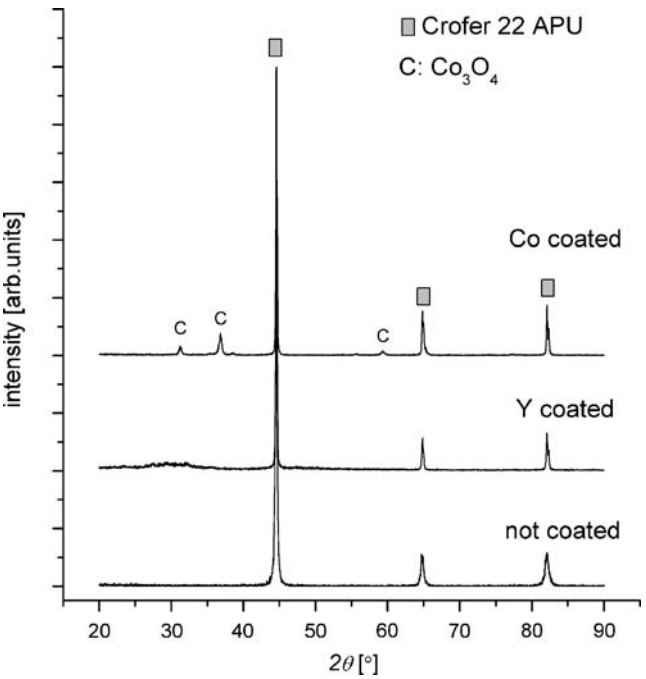

Fig. 2 XRD pattern of Y/Co-coated and uncoated samples fired at 380 °C

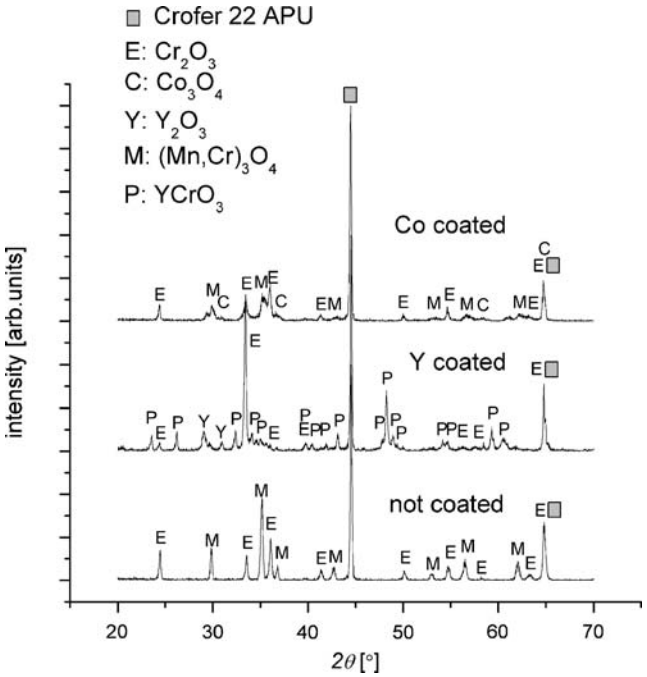

Fig. 3 XRD pattern of Y/Co-coated and uncoated samples fired at 800 °C for 562 h

from our previous studies [17]. Multiple coating procedure provides opportunity to tailor thickness of protective layers. In this study, precursors were deposited 15 times on each side, which yielded about 500-nm protective film.

Coated and uncoated samples were evaluated by cyclic thermogravimetry (TGA) and electrical conductivity measurements. The cyclic oxidation is probably more demanding for coatings than isothermal oxidation due to thermal stresses that arises upon heating and cooling process. However, cyclic oxidation is more realistic because SOFC need to survive many start ups. The cyclic thermogravimetry was performed in static atmospheric air in a muffle furnace at 800 °C. The coupons after initial weighting on a microbalance were placed in a furnace in such a manner that each side was exposed to air. After 3 h ramp time, they were held at 800 °C for a designated time and then were furnace-cooled (~3 h to cool down) to room temperature so they could be weighted. This procedure was performed several times until the total time of 562 h (162+200+200 h) was reached. Only time at soak temperature is taken into account.

The oxidation of alloys can be described by a thickness of the oxide scale that forms on the surface. When metal cation diffusion from bulk of the steel to the surface of the steel is a rate-limiting step of oxide scale formation, then the Wagner-like relationship is expected [18]:

$$\left(\frac{\Delta m}{A}\right)^2 = K_p \times t \tag{1}$$

where Δm—mass change of the steel after denoted time of oxidation (g), A—area of the sample (cm^2), K_p—parabolic rate law constant ($g^2\ cm^{-4}\ s^{-1}$), t—time (s).

An electrical conductivity of the oxide scale formed on coated and uncoated steel was measured using a four-terminal technique in a sandwich-like arrangement shown in Fig. 1. The platinum contacts were painted on the coupons, which were pre-oxidized for 40 h in a muffle furnace at 800 °C. Deposited platinum (ESL 5542) was fired at 750 °C for 30 min prior to any measurements. The contacts were in the form of 1 cm in diameter circles placed on opposite sides of the coupons. The coupons were spring-loaded in measurement cell, which provided good mechanical contact between sample and platinum mesh used as a current collector and a voltage probe. The measurement was performed using Keithley 2400 SourceMeter with a constant current density of ~380 mA cm^{-2}. The area-specific resistance (ASR) of oxide scale was calculated using equation:

$$\mathrm{ASR} = S\frac{R}{2} \tag{2}$$

where ASR—area-specific resistance ($\Omega\ cm^2$), S—contact area (cm^2), and R—measured resistance (Ω). A factor of 2 in Eq. 2 corresponds to a measurement setup in which a series connection of two identical resistances is measured on each side of a sample [12, 19].

X-ray patterns were obtained using the Philips X'Pert system. The surfaces of coupons were scanned at room temperature. The patterns were taken as standard 2θ scans. JCPDS-ICCD database was used for phase description.

Results and discussion

Prepared coatings were fully dense and well adhered to the steel. The grain size of deposited films fired at 800 °C is of ~20 nm.

Table 1 Summary of samples properties

Sample description	ASR at 800 °C ($m\Omega\ cm^2$)	Activation energy E_a (eV)	Parabolic rate constant K_p ($g^2\ cm^{-4}\ s^{-1}$)	Phases detected by XRD after TGA measurement
Crofer	10 (180 h)	0.91	2.84×10^{-14}	Cr_2O_3, $(Mn,Cr)_3O_4$
Crofer + Y	21 (212 h)	0.71	1.82×10^{-15}	Cr_2O_3, Y_2O_3, $YCrO_3$
Crofer + Co	76 (218 h)	0.75	2.06×10^{-14}	Cr_2O_3, Co_3O_4, $(Mn,Cr)_3O_4$

The X-ray diffraction (XRD) of the Y- and Co-coated samples taken right after firing at maximum processing temperature of 380 °C are shown in Fig. 2. For comparison, patterns of uncoated sample are included. It can be seen that yttrium coating is amorphous because any peak of the pattern can be attributed to Y_2O_3 (ICCD card number 20-1412). In contrary, the peaks corresponding to Co_3O_4 (ICCD card number 80-1535) are visible in the case of the cobalt-coated sample. This can be explained by different crystallization temperature of those precursor systems. At 600 °C, the films are transformed into crystalline oxides. Grain sizes of oxide films, which were calculated by Scherrer equation, are below 20 nm at 600 °C and below 100 nm at 1,000 °C.

The XRD patterns of samples fired for 562 h at 800 °C reveal more complicated structures (Fig. 3). The corresponding phase compositions are summarized in Table 1. In the case of the uncoated sample, the Cr_2O_3 (ICCD card number 11-0354) and the spinel $(Mn,Cr)_3O_4$ (ICCD card number 33-0892) are formed. Those phases are usually reported for this steel. The spinel structure forms on top of the chromia scale. In the case of the cobalt-coated sample, the same oxides and small traces of Co_3O_4 were found. In the case of the sample coated with yttrium, the Y_2O_3, Cr_2O_3, and a perovskite $YCrO_3$ (ICCD card number 34-365) are formed. There is not any manganese–chromium spinel visible in the pattern. Instead, chromium reacted with yttrium to form the perovskite. This type of behavior was previously reported for yttrium-coated 430 and 304 stainless steels [20–22]. The $YCrO_3$ is a perovskite that after doping (with Ca) was regarded as a ceramic interconnector material for high-temperature SOFCs. It has relatively high electrical conductivity of ~62 S cm^{-1} at 1,000 °C and low activation energy of 0.24 eV [23].

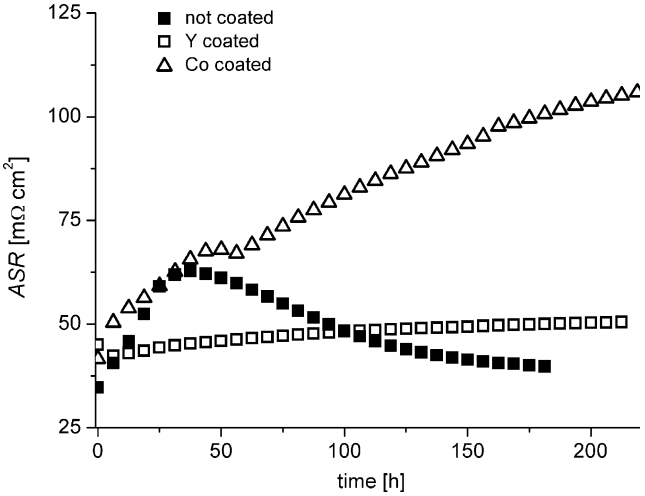

Fig. 5 Electrical conductivity of oxide scales as a function of oxidation time at 800 °C

Any spallation of oxide scale was not observed during cyclic thermogravimetry measurements of coupons, and therefore, it was possible to calculate coefficient K_p from the slopes in Fig. 4. Those values are presented in Table 1. It can be seen that the rate of oxidation is similar for uncoated and cobalt-coated samples. Much better coefficient is obtained for the yttrium coatings. In this case, the K_p value is of about one order of magnitude smaller than in other cases. The results cannot be directly compared with results reported by other groups due to cyclic (not isothermal) mode of the measurements. However, the K_p values in the case of the uncoated steel are consistent with isothermal results reported in [11]. The yttria coating reported in [11] resulted in lowered oxidation rate of steel. Namely, in the case of the yttria-coated samples, the rate of

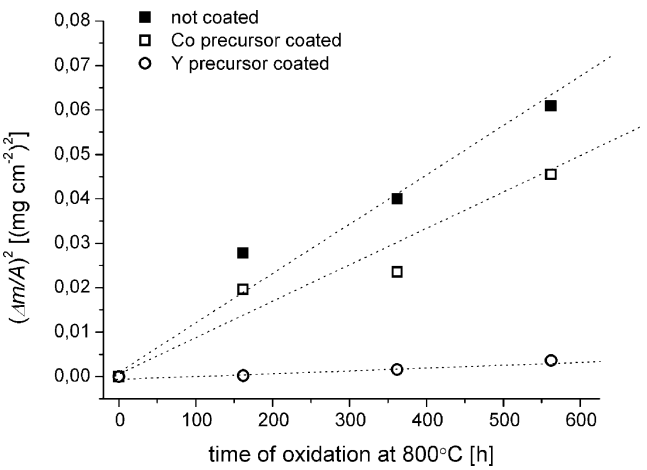

Fig. 4 Mass gain (parabolic units) of coupons as a function of time at 800 °C

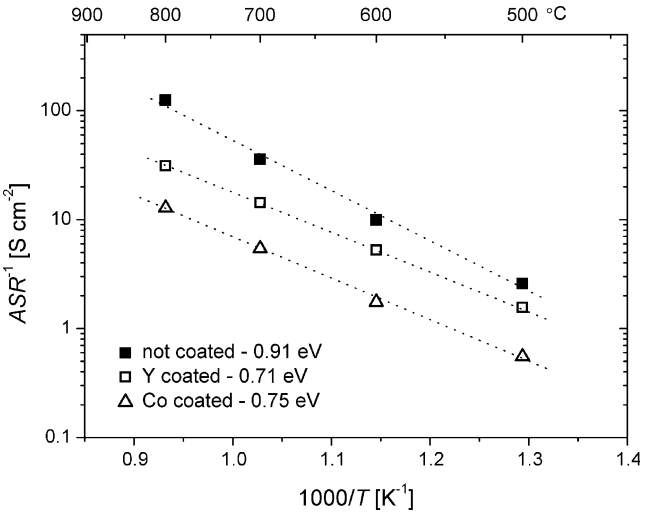

Fig. 6 The Arrhenius plot of area-specific resistance of coated and uncoated steel

oxidation K_p was estimated to be 1.1×10^{-14} (g^2 cm^{-4} s^{-1}) and was slightly lower than that of the uncoated. The thickness of yttria coating used in this study (~500 nm) is sufficient to protect steel from excessive oxide growth. Yttria has been previously shown [24] to have good adherence properties to metallic substrates. On the other hand, the prepared cobalt coating was probably too thin to form well adhered, mechanically stable, and continuous protective layer.

The electrical conductivity of the oxide scales measured in isothermal conditions at 800 °C is shown in Fig. 5. The uncoated sample has the lowest ASR. After initial rapid growth lasting ~45 h, the resistance decreased and stabilized at the level of 10 mΩ cm^2. This phenomenon can be related to formation of (Mn,Cr) protective spinel, which forms from initially created Cr_2O_3 oxide layer. The results are consistent with rapid decrease of ASR after 100-h oxidation of Crofer steel initially pre-oxidized for 100 h [13]. The samples coated with Co and Y show monotonic increase of ASR as a function of time, and the function seems to follow parabolic rate law. In the case of the Co coating, the ASR value is noticeably higher than in the case of the Y-coated sample. This can be correlated to TGA results in which the thickness of cobalt coating appears insufficient to protect steel. In addition, XRD showed that cobalt did not react with steel components because Co_3O_4 structure is remained. A continuous cobalt oxide film would have high electrical conductivity [9] so that ASR should remain low. Furthermore, when cobalt would react with manganese forming (Mn,Co) spinel, we would probably observe an improvement of ASR value which is observed for a deposited (Mn.Co) [16].

The ASR of oxide scale as a function of temperature in the range of 500–800 °C is presented in Fig. 6, and activation energies are summarized in Table 1. The activation energies of Co- and Y-coated steels (~0.7 eV) are comparable in value and lower than uncoated steel (~0.9 eV). The lowest activation energy is reported for Y coating (0.71 eV). Change of activation energy confirms different oxide scale composition. However, the activation energies of oxide scales cannot be compared directly to activation energy of pure chromia or yttria/cobalt coatings because the conductivity and activation energy are governed by other atoms present in steel, mainly Fe and Mn. Therefore, extrinsic behavior of those binary oxides is expected [4].

It is documented in the literature that yttrium additions improve oxide scale adherence and resistivity to thermal cycling. It also promotes selective oxidation of chromium and reduces fast diffusion of oxide scale components due to segregation into grain boundaries. The scale growth mechanism is changed from limiting outward metal cation diffusion into limiting inward oxygen anion diffusion [24].

Conclusions

In this paper, properties of a thin (~500 nm), nanocrystalline protective coatings of Y and Co on Crofer 22 APU were evaluated in respect to possible SOFC interconnect applications. It was shown that oxide scale growth is similar in the case of the uncoated and Co precursor coated sample. In the case of the Y precursor coated sample, the coating greatly reduces oxide scale formation. The electrical conductivity of Y-coated and uncoated samples are similar, while Co coating is higher. The XRD after long-term exposure at 800 °C shows formation of chromium oxide and Mn,Cr protective spinel for uncoated and Co-coated sample. In the case of the Y-coated samples, the $YCrO_3$ perovskite is formed. It may be concluded that yttria is more perspective for protective coating of the stainless steel than cobalt coating. However, it can be expected that the increase of Co thickness layer can improve mechanical and chemical stability of protective film.

Acknowledgment This work is supported by the project MNiSW 3 T10B 077 29. Thyssen Krupp VDM is acknowledged for supplying Crofer 22 APU free of charge.

References

1. Minh NQ, Takahashi T (1995) Science and technology of ceramic fuel cells. Elsevier, The Netherlands
2. Singhal SC, Kendall K (2003) High temperature solid oxide fuel cells. Fundamentals, design and application. Elsevier, The Netherlands
3. Minh NQ (2004) Solid State Ion 174:271 doi:10.1016/j.ssi.2004.07.042
4. Zhu WZ, Deevi SC (2003) Mater Res Bull 38:957 doi:10.1016/S0025-5408(03)00076-X
5. Fergus JW (2005) Mater Sci Eng A 397:271 doi:10.1016/j.msea.2005.02.047
6. Tucker MC, Lau GY, Jacobson CP, DeJonghe LC, Visco SJ (2007) J Power Sources 171:477 doi:10.1016/j.jpowsour.2007.06.076
7. Stanislowski M, Froitzheim J, Niewolak L, Quadakkers WJ, Hilpert K, Markus T et al (2007) J Power Sources 164:578 doi:10.1016/j.jpowsour.2006.08.013
8. Yang Z, Xia GG, Maupin GD, Stevenson JW (2006) J Electrochem Soc 153:A1852 doi:10.1149/1.2239371
9. Deng X, Wei P, Reza Bateni M, Petric A (2006) J Power Sources 160:1225 doi:10.1016/j.jpowsour.2006.03.024
10. Alman DE, Jablonski PD (2007) Int J Hydrogen Energy 32:3743 doi:10.1016/j.ijhydene.2006.08.032
11. Fontana S, Amendola R, Chevalier S, Piccardo P, Caboche G, Viviani M et al (2007) J Power Sources 171:652 doi:10.1016/j.jpowsour.2007.06.255
12. Belogolovsky I, Zhou XD, Kurokawa H, Hou PY, Visco S, Anderson HU (2007) J Electrochem Soc 154:B976 doi:10.1149/1.2756368
13. Yang Z, Xia GG, Maupin GD, Stevenson JW (2006) Surf Coat Technol 201:4476 doi:10.1016/j.surfcoat.2006.08.082
14. Yang Z, Xia G, Singh P, Stevenson JW (2006) J Power Sources 155:246

15. Brylewski T, Przybylski K, Morgiel J (2003) Mater Chem Phys 81:434 doi:10.1016/S0254-0584(03)00041-5
16. Gannon PE, Gorokhovsky VI, Deibert MC, Smith RJ, Kayani A, White PT et al (2007) Int J Hydrogen Energy 32:3672 doi:10.1016/j.ijhydene.2006.08.012
17. Jasinski P, Petrovsky V, Suzuki T, Petrovsky T, Anderson HU (2005) J Electrochem Soc 152:A454 doi:10.1149/1.1846711
18. Atkinson A (1985) Rev Mod Phys 57:437 doi:10.1103/RevModPhys.57.437
19. Piccardo P, Gannon P, Chevalier S, Viviani M, Barbucci A, Caboche G et al (2007) Surf Coat Technol 202:1221 doi:10.1016/j.surfcoat.2007.07.096
20. Riffard F, Buscail H, Caudron E, Cueff R, Issartel C, Perrier S (2002) Mater Charact 49:55 doi:10.1016/S1044-5803(02)00278-4
21. Qu W, Lia J, Ivey DG (2004) J Power Sources 138:162 doi:10.1016/j.jpowsour.2004.06.063
22. Qu W, Jian L, Ivey DG, Hill JM (2006) J Power Sources 157:335 doi:10.1016/j.jpowsour.2005.07.052
23. Tachiwakia T, Kunifusa Y, Yoshinaka M, Hirota K, Yamaguchi O (2001) Int J Inorg Mater 3:107 doi:10.1016/S1466-6049(01)00013-7
24. Chevalier S, Larpin JP (2002) Acta Mater 50:3105 doi:10.1016/S1359-6454(02)00106-4